

Effects of Cl⁻ concentration, temperature and AC interference on metastable pitting behavior of CoCrFeMnNi High-entropy alloy in a simulated concrete pore solution

Yanqi Zeng¹, Zhongping Le^{1,*}, Min Zhu^{1,*}, Li Liu², Jiayuan Shen³, Guotu Zhu⁴

¹ School of Mechanical Engineering & Automation, Zhejiang Sci-Tech University, Hangzhou 310018, China

² Interplex Electronic (HZ) Co., Ltd, Hangzhou 310018, China

³ Zhejiang Zheneng Natural Gas Operation Co., Ltd., Hangzhou 310052, China

⁴ Changshan Chengxin bearing Co., Ltd., Changshan 324000, China

*E-mail: zmii666@126.com, lelezp@126.com

Received: 4 September 2022 / Accepted: 9 October 2022 / Published: 20 October 2022

The metastable pitting corrosion behavior of CoCrFeMnNi HEA in a simulated concrete environment was studied under different factors by electrochemical measurements, statistics analysis method and scanning electron microscopy (SEM). The results show that the pitting corrosion resistance of the HEA under the impact of increasing Cl⁻ concentration, solution temperature and i_{AC} is weakened. The three factors promote the initiation and propagation of metastable pitting, and facilitate the evolution of metastable pitting to stable pitting. By comparing the data obtained by statistical analysis method, it can be concluded that the order of influence effect on the metastable pitting of the HEA is: solution temperature > AC interference > Cl⁻ attack.

Keywords: Metastable pitting, CoCrFeMnNi, Chloride ion, AC interference, Solution temperature

1. INTRODUCTION

High-entropy alloys (HEAs), a concept of designing alloys that typically consist of five or more prime elements in approximately equimolar concentrations, were first proposed by Yeh in 2004[1-3]. The HEAs usually show single solid solution phase with high mixing entropy [4-6]. Through the innovative design strategy of the alloys, HEAs exhibit sluggish diffusion, cocktail effects and severe lattice distortion [7-10]. Motivated by these effects, HEAs possess unparalleled mechanical properties, excellent phase stability and desired corrosion resistance [11-13]. As a result, HEAs have drawn considerable attention and have shown tremendous prospects in industrial applications.

Among various HEAs, the equiatomic CoCrFeMnNi HEA with the unique face-centered-cubic (FCC) structure has been widely studied since its superior mechanical properties and corrosion resistance [14-21]. For instance, Zhang [22] evaluated the influence of thermal shock irradiation on the mechanical properties of CoCrFeMnNi HEA, which exhibited better resistance to irradiation cracking than tungsten (w). Kim [23] investigated the high-cycle fatigue (HCF) behavior of coarse-grained CoCrFeMnNi HEA, and the result confirmed that the yield strength, tensile strength, elongation and the HCF strength were 293.1 MPa and 625.6 MPa, 63.1% and 280 MPa, respectively. Xu [24] fabricated the CoCrFeMnNi HEA by additive manufacturing using selective laser melting (SLM), and compared the corrosion resistance of SLMed with as-cast HEAs, where the passive film produced on SLMed HEA was more stable. Luo [25] investigated the corrosion behavior of the HEA and 304 L SS in 0.1 M H₂SO₄ solution, and the X-ray photoelectron spectroscopy (XPS) results verified that the passive film formed on the HEA was slightly thicker than that on the 304L SS. Thus, CoCrFeMnNi HEA exhibits an extensive potential to be an alternative candidate material employed in engineering field. Reinforced concrete is most widely used in practical buildings [26-30]. It is well known that reinforcement corrosion is one of the primary reasons affecting the lifetime and the expectancy of reinforced concrete structures [31-35]. Consequently, it is necessary to study the corrosion behavior of CoCrFeMnNi HEA as the potential rebar in a simulated concrete pore solution.

Numerous research and our previous studies demonstrated that pitting corrosion was generally initiated on CoCrFeMnNi HEA in neutral, acidic and slightly alkaline environments [21,25,36-39]. In addition, Luo [40] found that the HEA suffered from pitting corrosion in chlorinated concrete pore solution. From these literature, it could be concluded that pitting corrosion is the primary corrosion form of CoCrFeMnNi HEA in various environments. It is generally accepted that the metastable pitting is the early stage of stable pitting, and the growth of metastable pitting determines whether stable pitting is formed [41-45].

In the practical application of concrete structure, the contributing factors to reinforced steel corrosion include chloride concentration, environmental temperature and alternating current (AC) interference [46-54]. Moreover, the corrosion behavior of rebar subjected to AC interference and environmental temperature may become complicated by the presence of chloride ion [55-57]. However, at present, there are no reports on the metastable pitting behavior of the HEA. Hence, it is worth studying the influences of Cl⁻, solution temperature and alternating current (AC) interference on the metastable pitting corrosion behavior of CoCrFeMnNi HEA in a simulated concrete pore solution.

2. EXPERIMENTAL

2.1. Material and solution

Ingots of equiatomic CoCrFeMnNi HEA with a chemical composition (21.3Co, 19.6Cr, 18.4Fe, 20.5Mn, 20.2Ni, wt.%) were prepared at a melting temperature of 1700 °C under an inert gas atmosphere in an induction suspension furnace, and the purity for each metal raw in the HEA was above 99.9%. Two samples with different sizes were machined from the cast ingots. The specimen

with a larger exposed surface area of 10 mm × 10 mm was used for potentiodynamic polarization measurement. To reduce the overlap of current fluctuations, the sample with small surface area of 1 mm × 1 mm was employed for potentiostatic polarization test. To avoid unnecessary crevice corrosion occurred at specimen/epoxy interface during electrochemical experiments, the back side of each specimen was soldered to a copper wire and then packaged with epoxy resin. Prior to testing, the specimen surface was wet-abraded with sandpapers from 320 to 2000 grit, followed by polishing with 0.5 μm diamond paste. Then, the polished sample was ultrasonically rinsed with alcohol and deionized water, and air-dried. The microstructure of the HEA was etched with aqua regia for 5 seconds, and observed by scanning electron microscopy (SEM, FEI Quanta 250). As displayed in Fig. 1, the CoCrFeMnNi HEA consists of a single FCC structure, with various size grains.

The simulated concrete pore solution was 0.001 M Ca(OH)₂+0.2 M NaOH+0.6 M KOH [58,59].

2.2 Electrochemical tests

The electrochemical tests were undertaken at the CHI660E electrochemical workstation with a classical three-electrode cell system. A saturated calomel electrode (SCE) was adopted as the reference electrode (RE) and a platinum (Pt) sheet was employed as the counter electrode (CE). In addition, the HEA sample was used as the working electrode (WE). Prior to the potentiodynamic polarization curve test, the samples were immersed in the corresponding solutions for 1.5 h. The polarization curves were measured at a sweep rate of 1 mV/s with a potential range of -1 V (vs. SCE) ~ 0.7 V (vs. SCE). To explore the effects of Cl⁻, temperature and AC interference on the behavior of metastable pitting corrosion, the potentiostatic polarization curve test was performed at 0.3 V_{SCE} for 0.5 h. The potential was selected from the potentiodynamic polarization curves (Fig.2). The specific experimental design was as follows:

To study the influence of chloride ion on the metastable pitting corrosion of the MEA, all electrochemical curves were measured at 30 °C in the simulated concrete pore solution containing various NaCl concentrations of 0, 0.15 and 0.50 M. With respect to the solution temperature, the electrochemical tests were performed in the simulated concrete pore solution with 0.15M Cl⁻ at different temperatures of 30 °C, 40 °C and 50 °C. For AC interference, various i_{AC} of 0, 3, 5 and 8 A/m² were applied to the samples, and the AC frequency was 50 Hz. The AC current density in this work was root-mean-square value, which was measured by a clamp meter. The testing setup for obtaining the electrochemical curves under applied AC was consistent with our previous literature [60,61]. The related test was achieved in the simulated concrete pore solution with 0.15M Cl⁻ at 30 °C. Each test was repeated four times to ensure reproducibility. It was pointed out that various low i_{AC} were applied to the HEA electrode in the metastable pitting study, whereas different relatively high i_{AC} of 0, 30, 50 and 80 A/m² were imposed in the potentiodynamic polarization test. This is due to the fact that the metastable transient information can not be clearly exhibited because the application of large i_{AC} produces intense polarization and causes the initiation of steady-state pitting.

2.3. Metastable pitting characterization

Morphology characterization of metastable pitting corrosion was observed by SEM. The metastable pitting was generated by potentiostatic polarization at 0.3 V_{SCE} in the simulated concrete pore solution containing 0.5 M Cl⁻.

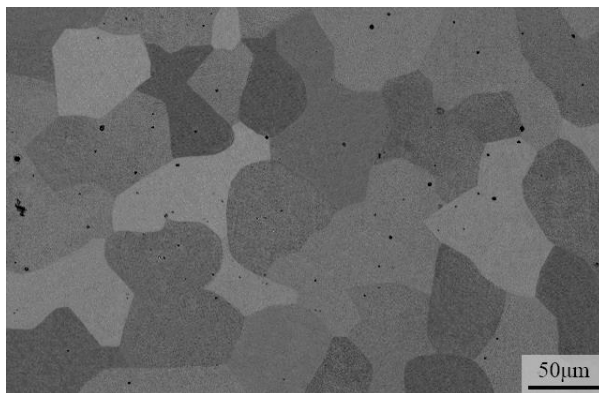
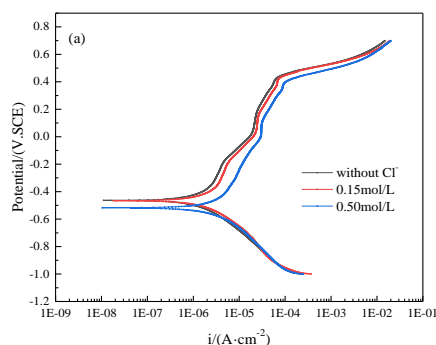


Figure 1. Microstructure of CoCrFeMnNi HEA.

3. RESULTS

3.1. Potentiodynamic polarization curve

Fig. 2 depicts the potentiodynamic polarization curves of CoCrFeMnNi HEA under different testing conditions. All curves show similar passive characteristics. As Cl⁻ concentration, AC current density and solution temperature increase, the polarization curves move to the right, which means that the corrosion current density increases. The phenomenon implies that the accumulation and adsorption of Cl⁻ and other aggressive ions on the electrode surface increases the degree of local destruction of passive film, causing an increase in the number of active sites and accelerated anodic dissolution.



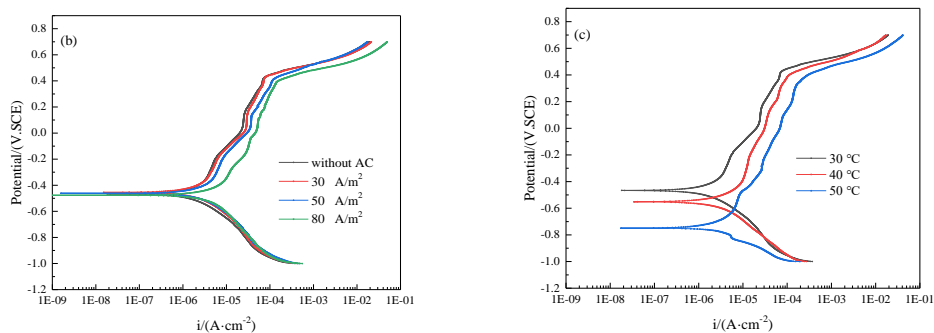


Figure 2. Potentiodynamic polarization curves of CoCrFeMnNi HEA in simulated concrete pore solution with: (a) different Cl^- concentrations at 30 °C; (b) 0.15 M Cl^- at different AC current densities and 30 °C; (c) 0.15 M Cl^- at different solution temperatures.

The fitting values of passive current density (i_p) and pitting potential (E_p) can be derived from the polarization curve, as exhibited in Fig. 3. With the increase of Cl^- concentration, AC current density and solution temperature, i_p increases and E_p moves in the negative direction. Larger i_p value indicates the formation of a more fragile or porous passive film on the surface of the HEA, which is less protective and stable [62]. As for the variation of E_p , it can be inferred that the sensitivity to pitting corrosion is enhanced. The change trend of the two parameters in Fig. 3 reveals that the anti-corrosion resistance of the HEA under the impact of these factors is weakened. Moreover, the corrosion potential (E_{corr}) decreases with increasing Cl^- concentration and solution temperature, which denotes a higher electrochemical activity and a stronger tendency for active corrosion.

As Cl^- concentration increases, the presence of Cl^- makes the HEA susceptible to disruption of the passive film. The curves measured under imposed AC (Fig. 2b) reveal that the electrochemical activity of the HEA is promoted, leading to a faster dissolution rate to break the equilibrium state between the formation and dissolution of passive film. In contrast, a more pronounced variation in the electrochemical parameters of i_p and E_{corr} is exhibited, signifying that the acceleration effect of solution temperature on the corrosion of the HEA is greater than those of AC application and Cl^- attack. Solution temperature affects the thermodynamic state and kinetic process during the occurrence of electrochemical corrosion: at higher solution temperatures, the activity of Cl^- is greatly improved, thus more Cl^- ions adsorb on the surface of passive film, and the active region on the film is expanded. Hence, it is difficult for the metal to establish and maintain a stable passive state. Furthermore, the stability and repair ability of the passive film decrease, which causes the pitting resistance of the HEA to be weakened.

In potentiodynamic polarization test, stable pitting is occurred at anodic potential above E_p , while metastable pitting is produced at potentials slightly below E_p . To characterize the metastable pitting corrosion behavior related to Cl^- attack, AC interference and solution temperature, specimens were polarized at a constant potential below E_p . According to the curves in Fig.2, the potential for potentiostatic polarization test was chosen to be 0.3 V_{SCE} .

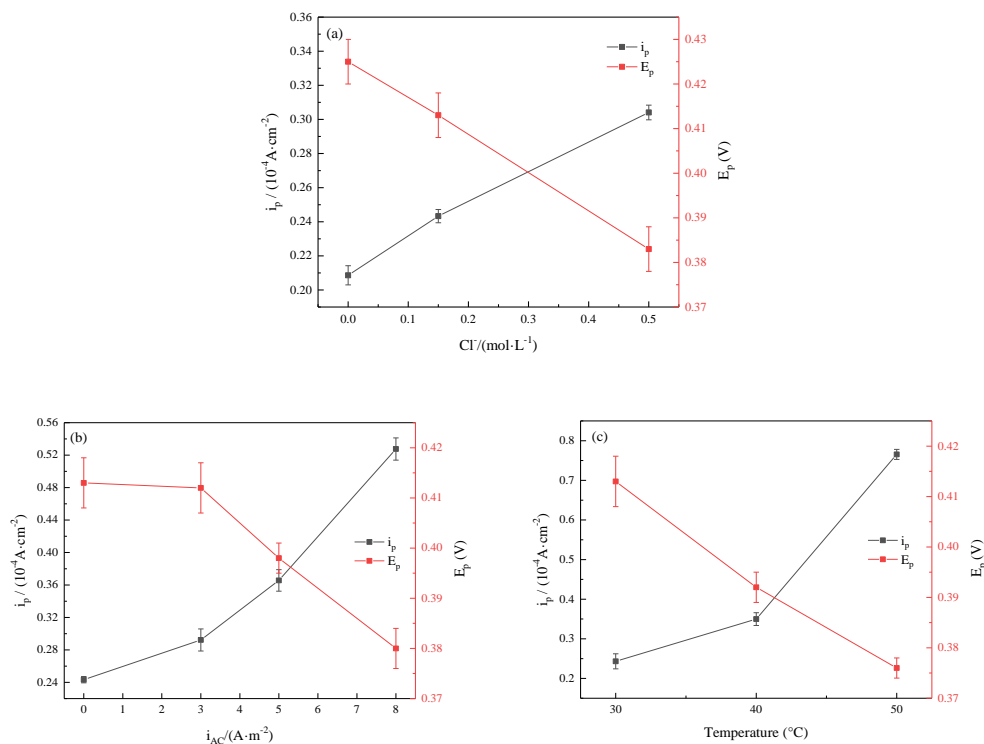
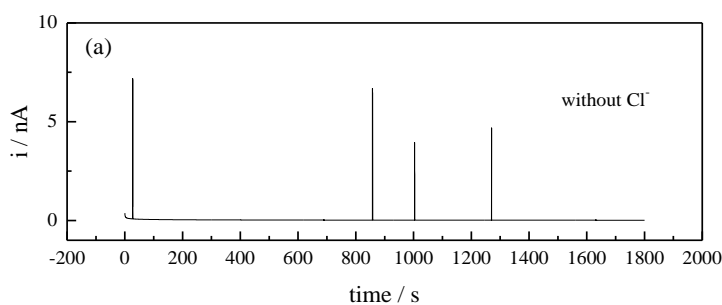


Figure 3. Variation in corrosion parameters extracted from the potentiodynamic polarization curves of CoCrFeMnNi HEA in simulated concrete pore solution with: (a) different Cl^- concentrations at 30 $^{\circ}\text{C}$; (b) 0.15 M Cl^- at different AC current densities and 30 $^{\circ}\text{C}$; (c) 0.15 M Cl^- at different solution temperatures.

3.2. Metastable pitting analysis

Fig. 4 displays the variation of current-time transient curves measured in simulated concrete pore solutions with various Cl^- concentrations. It is noteworthy that visible transient current peaks can be observed, which corresponds to the rupture and repair of the passive film and is an indicator of the metastable pitting trend [45]. The results show that the amplitude and frequency of the metastable pitting current density peak increase with Cl^- concentration. This suggests that Cl^- attack accelerates the nucleation and growth of metastable pits, which ultimately increases the probability of generation of metastable pits..



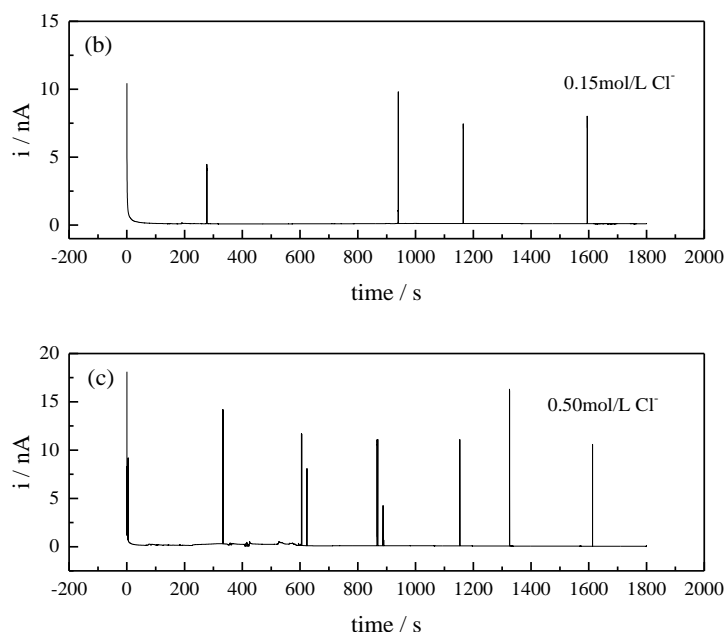


Figure 4. Potentiostatic polarization curves of CoCrFeMnNi HEA under 0.3 V_{SCE} in simulated concrete pore solution containing different Cl^- concentrations at 30 °C: (a) without Cl^- , (b) 0.15 mol/L and (c) 0.50 mol/L.

There exist two types of anodic current density peaks during the occurrence of metastable pits, as presented in Fig. 5a-c. The type 1 in Fig. 5a is composed of a slow increase in current followed by a sharp drop. The relatively slow rise in current is induced by the anodic dissolution of the HEA surface, while the rapid fall corresponds to the repassivation of metastable pitting [63]. Thus, the kinetic processes of metastable pitting can be extracted from the type 1, including initiation, propagation and repassivation of metastable pits. The type 2 is characterized by a shape of a sudden rise and fast decay in current, as described in Fig. 5b. The type 2 in current is ascribed to no propagation of metastable pitting corrosion. As observed in Fig. 5a, the parameters are defined to illustrate the metastable pitting process [64-67], where i_{bg} is background current density, i_{peak} is peak current density ($i_{max} - i_{bg}$), t_0 and t_2 are the initiation time and the repassivation end time of metastable pitting, and t_1 is the time to peak. $t_{grow}(t_1 - t_0)$, $t_{rep}(t_2 - t_1)$, and $t_{lifetime}(t_2 - t_0)$ are the growth time, repassivation time, and lifetime of an individual metastable pitting, respectively.

In Fig. 4, different types of metastable pitting current density peaks (single-peak transients and overlapped-peak transients) appear in the statistical process of current density peaks. The single peak contains only one rising and dropping current and its change process is without secondary pitting (Fig. 5b), and the overlapped peak includes two or more peaks, as displayed in Fig. 5c. This may be attributed to the exposure of sulfur-containing inclusion around the metastable pitting, which may induce multiple pitting nucleation, resulting in overlapped current peaks [45]. To deeply investigate the effects of different factors, statistical analysis was performed. Before analyzing the data, the background current density (i_{bg}) of the HEA was determined to be 3.2 $nA \cdot cm^2$ by potentiostatic polarization test in Na_2SO_4 solution. In the polarization process, there is no pitting generated on the HEA. When the peak current density value is larger than i_{bg} , it is counted as the metastable pitting peak.

For overlapped peak, when its current density declines by less than 50 %, a new peak produces, which is regarded as the same metastable pitting. Conversely, the new peak is considered to be a new metastable pit.

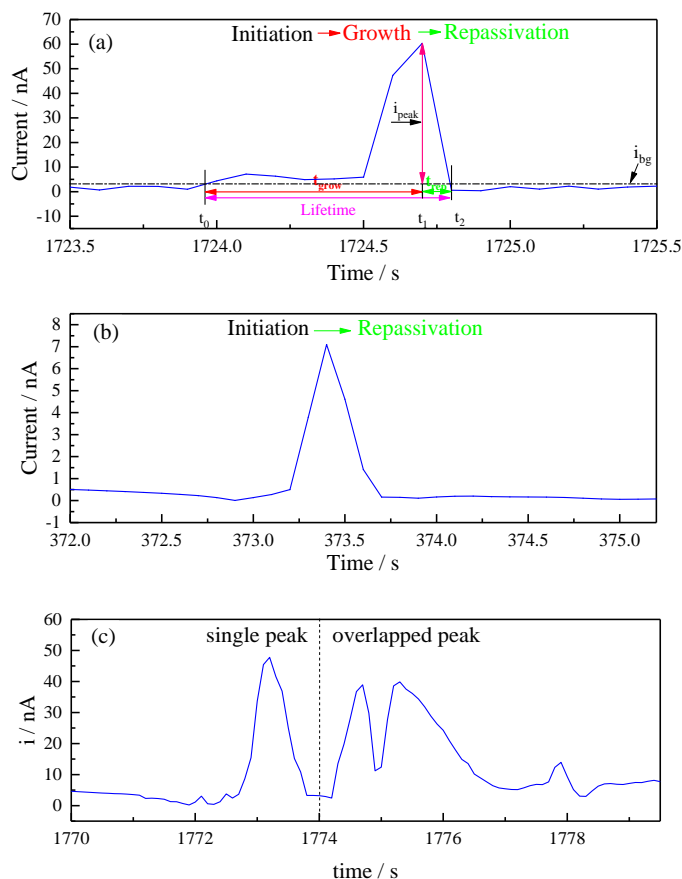


Figure 5. Current peaks (single peak transient and overlapped peaks transient) of metastable pitting of CoCrFeMnNi HEA in simulated concrete pore solution.

3.3. Effect of chloride ion on metastable pitting

The statistical result of Fig. 4 can quantitatively reflect the change in the kinetics of metastable pitting. More details concerning the i_{peak} , $t_{Lifetime}$ and average metastable pit number density (N_{avg}) of current-time transients measured under different conditions are discussed. Fig. 6 illustrates the i_{peak} , $t_{Lifetime}$ and number of metastable pitting of the HEA extracted from Fig. 4. The values of i_{peak} , N_{avg} and $t_{Lifetime}$ of metastable pitting increase with the increase of Cl^- concentration. This implies that the propagation of metastable pitting easily occurs at higher Cl^- concentration. The i_{peak} value is proportional to the activation energy of metastable pitting. And the high activation energy of metastable pitting can trigger the formation of deeper pit cavity, which provides a more efficient space to facilitate the pit expansion. The average $t_{Lifetime}$ value directly reflects the speed of pit initiation, growth and repassivation. With the prolongation of average $t_{Lifetime}$, the metastable pitting formed on

the HEA surface can extend continuously and prevent repassivation of the HEA, resulting in an enhancement of transformation probability of stable pitting. The change trend of maximum t_{Lifetime} also indicates that the metastable pit may become larger with the increase of Cl^- concentration. This implies that the repassivation capacity of the HEA specimen decreases with the increase of Cl^- concentration. This may be due to the fact that Cl^- penetrates through the passivation film and combines with the matrix metal ions during the process of pitting initiation.

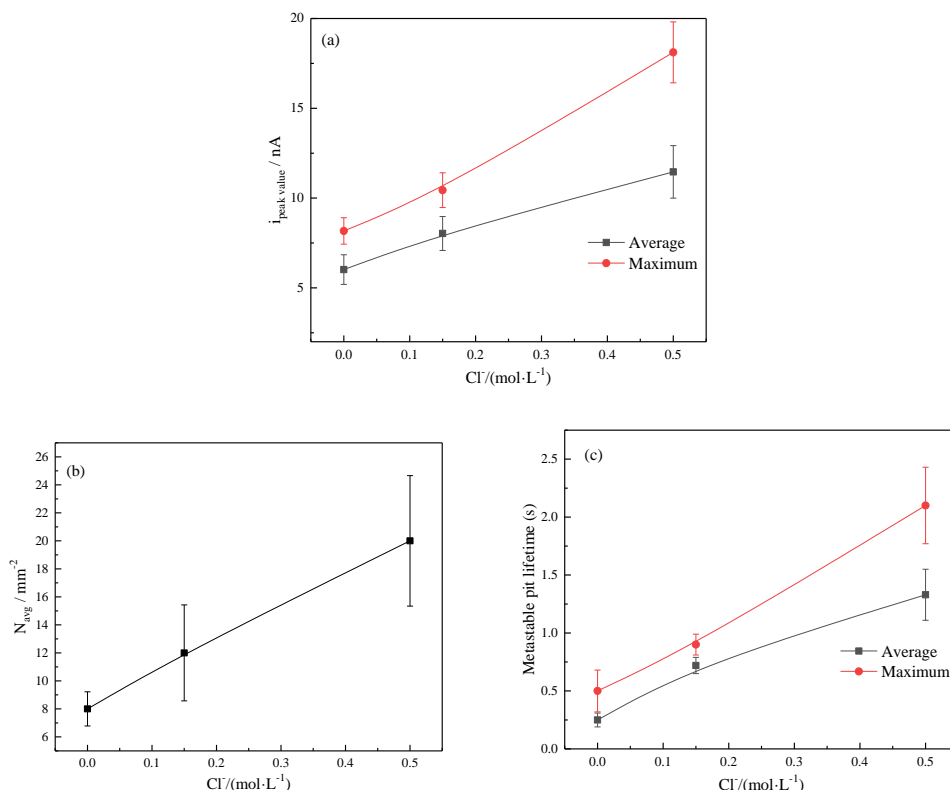


Figure 6. The extracted corrosion parameters from the potentiostatic polarization curves of CoCrFeMnNi HEA in simulated concrete pore solution containing various Cl^- concentrations at 30 °C: (a) i_{peak} value, (b) average metastable pit number density and (c) lifetime.

The produced metal chlorides reduce the pH inside the pitting through hydrolysis, while oxygen-containing ions are difficult to form metal oxides in local acidic environment in interior of pits, so it is easy to form autocatalytic acidification at higher concentration of Cl^- -containing solution when metastable pitting erupts, which promotes the rapid development of pitting, and reduces the possibility of repassivation in the pit [68]. N_{avg} at a lower level corresponds to the fewer nucleation frequency and propagation of metastable pit. As N_{avg} value increases, the passive film possesses more active sites and the rupture of the film occurs more frequently. The ionic conductivity of the passive film is enhanced by the increase in Cl^- concentration, resulting in a strong ion-induced conductor on the metal electrode surface where the film is defective, which causes an increase in the frequency of transient current peaks with a sudden increase in current density. According to passive film theory, when Cl^- or chloride complex ions are replaced with stable oxide ions in the passive film, the film at that point is destroyed

and the base metal is exposed to form a corrosion nucleus. Therefore, when Cl^- concentration increases, the probability of pitting corrosion germination increases [69].

During the forming process of corrosion pit, the anions and metal cations inside pitting generally keep dynamic balance. However, with the increase of Cl^- concentration in the solution, the diffusion of metal cations is accelerated. The metal cations are continuously dissolved into the solution, and hydrolyzed, which increases the acidity of local environment inside the pit. Additionally, the accumulation of Cl^- on the surface of electrode and the increase of chemisorption aggravate the damage degree of the passive film[70], which can generate more active spots on the surface of HEA. Thus, increasing Cl^- concentration promotes the production of metastable pitting. Fig. 7 displays the metastable pitting morphology of CoCrFeMnNi HEA after potentiostatic polarization at $0.3 \text{ V}_{\text{SCE}}$ for 0.5 h in simulated concrete pore solution containing 0.5 M Cl^- . The isolated and small metastable pits are observed on the surface of the HEA.

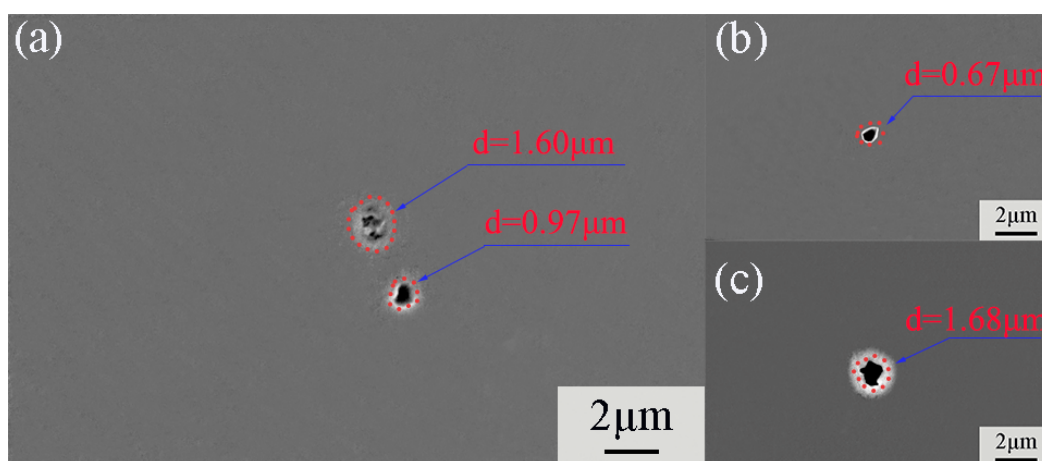


Figure 7. Morphology of metastable pitting of CoCrFeMnNi HEA under $0.3 \text{ V}_{\text{SCE}}$ in simulated concrete pore solution containing 0.5 M Cl^- at $30 \text{ }^\circ\text{C}$.

3.4. Effect of AC interference on metastable pitting

Fig. 8 exhibits the current-time transient curves of the HEA under various i_{AC} interference in simulated concrete pore solution containing 0.15 M Cl^- . Clearly, both the occurrence frequency and current amplitude of metastable pitting increase with applied i_{AC} . According to aforementioned statistical analysis method, the analysis results are presented in Fig. 9, which shows an upward trend. This implies that AC interference causes an adverse effect on the occurrence of metastable pitting of the HEA. Known from the previous literature [39,60,61], the application of AC can cause current fluctuation, resulting in the generation of hydrogen atom and an increase in the electrochemical activity of metals. Upon application of AC, the adsorption rates of corrosive chloride ion and hydrogen atom on the defects of passive film are enhanced, which promotes the occurrence of metastable pitting.

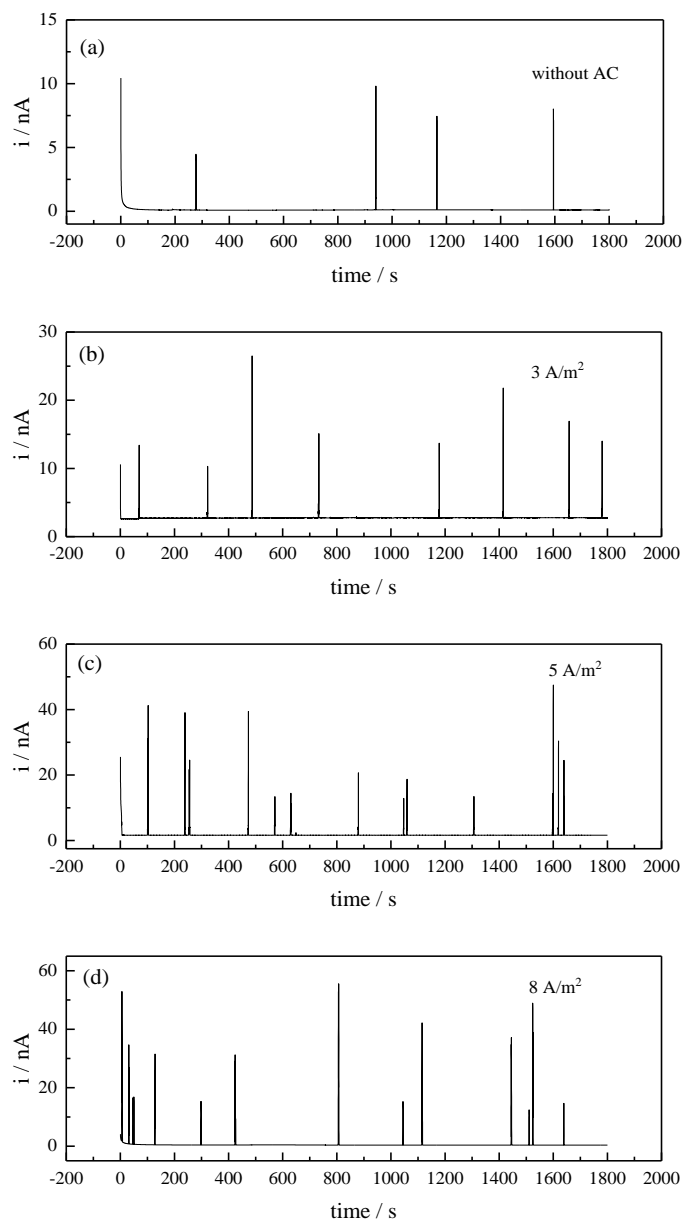
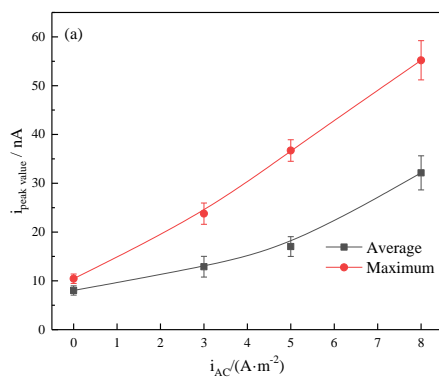


Figure 8. Potentiostatic polarization curves of CoCrFeMnNi HEA under 0.3 V_{SCE} in simulated concrete pore solution containing 0.15 M Cl^- interfered at various i_{AC} and $30 \text{ }^\circ\text{C}$: (a) without AC, (b) 3 A/m^2 , (c) 5 A/m^2 , and (d) 8 A/m^2 .



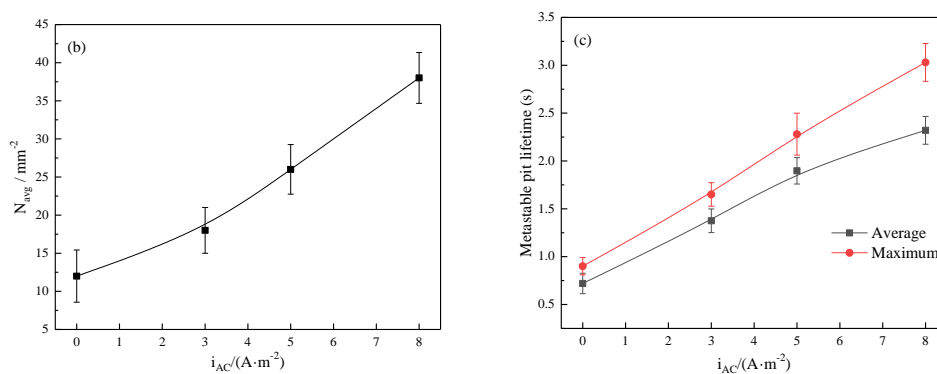
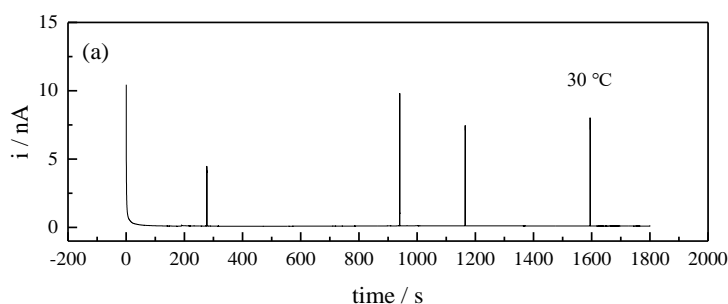


Figure 9. The extracted corrosion parameters from the potentiostatic polarization curves of CoCrFeMnNi HEA in simulated concrete pore solution containing 0.15 M Cl^- interfered at different i_{AC} and 30 °C: (a) i_{peak} , (b) average metastable pit number density and (c) lifetime.

Especially at a higher i_{AC} value, AC facilitates the migration of various ions due to the electric field [71], which shortens the distance of ion collision and increases the speed of reaction, prompting the generation of metastable pitting (Fig. 9b). Additionally, the alternating electric field generated by AC has an essential influence on the metastable pitting behavior of the HEA. When AC current is applied, the HEA is in the alternating process of anodic and cathodic polarization. Among them, anodic polarization accelerates the anodic dissolution process of the metal, while cathodic polarization slows down the occurrence of corrosion [72]. The positive half-cycle of alternating current makes the surface of the specimen occur oxidation reaction, such as Fe^{2+} is oxidized into Fe^{3+} . In AC negative half-cycle, reduction reaction is occurred on the electrode surface, such as Fe^{3+} is reduced to Fe^{2+} . As the AC density increases, the anodic oxidation effect of the specimen is more obvious than that of cathodic reduction. Accordance with the adsorption theory of passive film, the pitting is attributable to the adsorption of corrosive anions on the surface of the film, and then the ions pass through the film. Under applied AC, the film is in a dynamic equilibrium of continuous dissolution and repair. And Cl^- can preferentially and selectively adsorb on the film surface to crowd out the oxygen atoms, thus combining with the cations in the film to form soluble chlorides that expose the fresh metal surface and create pitting [73]. The above results indicate an increase in the generation rate of metastable pitting of the HEA.

3.5. Effect of temperature on metastable pitting



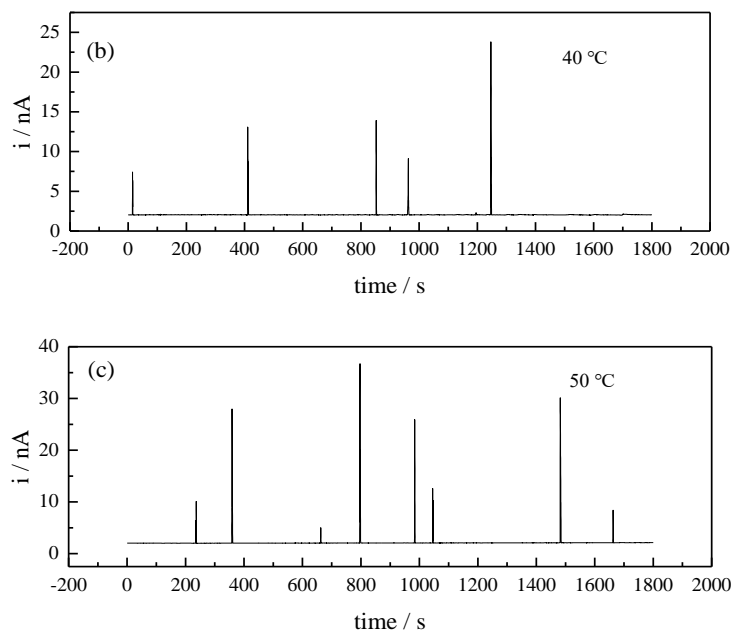


Figure 10. Potentiostatic polarization curves of CoCrFeMnNi HEA under $0.3 V_{SCE}$ in simulated concrete pore solution containing $0.15 M Cl^-$ concentration at various temperatures: (a) $30 ^\circ C$, (b) $40 ^\circ C$ and (c) $50 ^\circ C$.

As shown in Fig. 10, the amplitude and number of metastable pitting current peak increase with the increase of solution temperature. All curves in Fig. 11 exhibits the analogous growing tendency. This demonstrates that the increasing solution temperature facilitates the formation of metastable pitting. In fact, temperature affects the diffusion rate of ions. As the temperature increases, the reaction driving force intensifies, and the migration rate of chloride ions increases, which accelerates the metal dissolution[74]. In addition, with the increase in solution temperature, the oxygen in the solution is easy to escape, which can inhibit the corrosion.

On the one hand, the increase in temperature accelerates the dissolution of passive layer on the HEA surface; on the other hand, the reformation of passive layer on the bare surface of metals is promoted. But the former process is faster than the latter, so the rise in temperature leads to thinner passive layer produced on the surface of the HEA [75]. Moreover, rising temperature increases the activation energy of the metal surface, which increases the number of surface active spots and the tendency to form metastable pitting. Furthermore, an increase in temperature accelerates the diffusion of H^+ and Cl^- , which hinders the formation of the passive film and promotes the development of the pitting. Additionally, rising temperature enhances the autocatalytic reaction on the HEA surface and facilitates the destruction of surface passive film [76].

Known from Fig.6, 9 and 11, by comparing the data obtained by statistical analysis method, it can be concluded that the order of influence effect on the metastable pitting of the HEA is: solution temperature > AC interference > Cl^- attack.

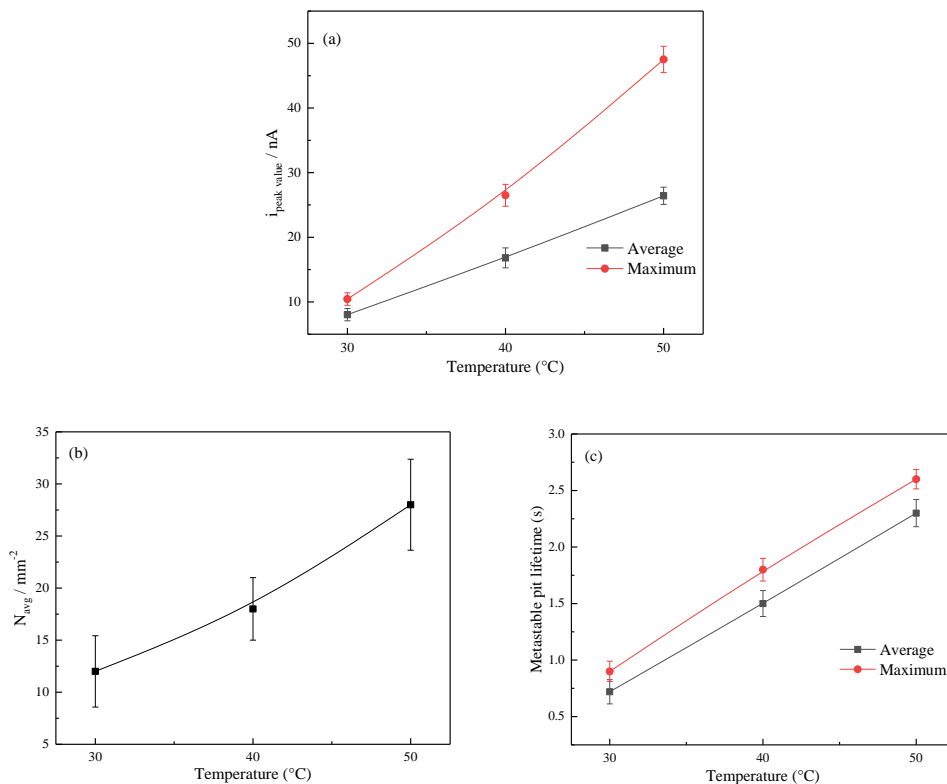


Figure 11. The extracted corrosion parameters from the potentiostatic polarization curves of CoCrFeMnNi HEA in simulated concrete pore solution containing 0.15 M Cl⁻ at different temperatures of 30, 40 and 50 °C: (a) i_{peak} value, (b) average metastable pit number density and (c) lifetime.

4. CONCLUSIONS

In this study, the metastable pitting behavior of CoCrFeMnNi HEA under various factors of Cl⁻ concentration, AC current density and solution temperature was studied in a simulated concrete pore solution. The main conclusions are outlined below:

- 1) The pitting corrosion resistance of the HEA under the impact of increasing Cl⁻ concentration, solution temperature and i_{AC} is weakened. The acceleration effect of solution temperature on the corrosion of the HEA is greater than those of AC application and Cl⁻ attack.
- 2) The increased Cl⁻ concentration, solution temperature and i_{AC} promote the initiation and propagation of metastable pitting, and facilitate the transition of metastable pitting to stable pitting.
- 3) By comparing the data obtained by statistical analysis method, it can be concluded that the order of influence effect on the metastable pitting of the HEA is: solution temperature > AC interference > Cl⁻ attack.

ACKNOWLEDGEMENTS

This work was supported by the National Natural Science Foundation of China (No. 51871026) and National Material Environmental Corrosion Infrastructure.

References

1. N.B. Hua, W.J. Wang, Q.T. Wang, Y.X. Ye, S.H. Lin, L. Zhang, Q.H. Guo, J. Brechtel and P.K. Liaw, *J. Alloys Compd.*, 861(2021)157997.
2. C. Chen, J.L. Chen, S.H. Yuan, W.Z. Li, W. Wang, X.F. Li, W.W. Zhang, R. Wei, S.K. Guan, T. Wang, T. Zhang, N. Lei and F.S. Li, *J. Alloys Compd.*, 8(2022)163714.
3. C. Cui, M.P. Wu, X.J. Miao, Z.S. Zhao and Y.L. Gong, *J. Alloys Compd.*, 890(2022)161826
4. Z.J. Zhang, E.H. Han and C. Xiang, *Corros. Sci.*, 191(2021)109742.
5. P.F. Wu, K.F. Gan, D.S. Yan, Z.H. Fu and Z.M. Li, *Corros. Sci.*, 183(2021)109341.
6. Y. Garip, N. Ergin and O. Ozdemir, *J. Alloys Compd.*, 877(2021)160180.
7. J. Xu, S. Peng, Z.Y. Li, S.Y. Jiang, Z.H. Xie, P. Munroe and H. Lu, *Corros. Sci.*, 190(2021)109663.
8. H. Shi, R. Fetzer, A. Jianu, A. Weisenburger, A. Heinzl, F. Lang and G. Müller, *Corros. Sci.*, 190(2021)109659.
9. Y. Guo, L. Liu, W. Zhang, K. Yao, Z.F. Zhao, J. Shang, J.G. Qi, M.H. Chen, R.D. Zhao and F.F. Wu, *J. Alloys Compd.*, 889(2021)161676.
10. Y.T. Lou, C.D. Dai, W.W. Chang, H.C. Qian, L.Y. Huang, C.W. Du and D.W. Zhang, *Corros. Sci.*, 165(2020)108390.
11. M.J. Li, Q.J. Chen, X. Cui, X.Y. Peng and G.S. Huang, *J. Alloys Compd.*, 857(2021)158278.
12. P. Moazzen, M.R. Toroghinejad, T. Zargar and P. Cavaliere, *J. Alloys Compd.*, 892(2021)161924.
13. S. Yadav, Q.F. Zhang, A. Behera, R.S. Haridas, P. Agrawal, J.D. Gong and R.S. Mishra, *J. Alloys Compd.*, 893(2022)162265.
14. J.B. Li, B. Gao, Y.T. Wang, X.H. Chen, Y.C. Xin, S. Tang, B. Liu, Y. Liu and M. Song, *J. Alloys Compd.*, 792(2019)170.
15. X.B. Guo, I. Baker, F. E. Kennedy, S. P. Ringer, H.S. Chen, W.D. Zhang, Y. Liu and M. Song, *Mater. Charact.*, 170(2020)110693.
16. Z.L. Xu, H. Zhang, W.H. Li, A.Q. Mao, L. Wang, G.S. Song and Y.Z. He, *Addit. Manuf.*, 28(2019)766.
17. Y.F. Wang, L. Xia, Y.T. Cao, H.J. Zhang, Z.H. Hao and W.C. Wu, *Mater. Sci. Eng. A*, 793(2020)139893.
18. J.M. Park, E.S. Kim, H. Kwon, P. Sathiyamoorthi, K.T. Kim, J.H. Yu and H.S. Kim, *Addit. Manuf.*, 47(2021)102283.
19. Y.K. Kim, J. Choe and K.A. Lee, *J. Alloys Compd.*, 805(2019)680.
20. S. Picak, H.C. Yilmaz and I. Karaman, *Scr. Mater.*, 202(2021)113995.
21. L. Pao, I. Muto and Y. Sugawara, *Corros. Sci.*, 191(2021)109748.
22. L.S. Zhang, X.N. Zhang, N. Li, X.X. Mei, X.N. Li, Y.N. Wang, X.Z. Cao, S. K. Pavlov, G.E. Remnev, V.V. Uglov and E. Lu, *J. Nucl. Mater.*, 17(2021)153413.
23. Y.K. Kim, G.S. Ham, H.S. Kim and K.A. Lee, *Intermetallics*, 111(2019)106486.
24. Z.L. Xu, H. Zhang, X.J. Du, Y.Z. He, H. Luo, G.S. Song, L. Mao, T.W. Zhou and L.L. Wang, *Corros. Sci.*, 177(2020)108954.
25. H. Luo, Z.M. Li, A.M. Mingers and D. Raabe, *Corros. Sci.*, 134(2018)131.
26. M.Y. Hang, M.H. Jiang, W.L. Zhao, Y.B. Yang and T. Cheng, H. Wang, *J. Build. Eng.*, 44(2021)103221.
27. L.Z. Dai, D.X. Long and L. Wang, *Comput. Struct.*, 254(2021)106615.
28. B. Baten, T. Manzur, T. Torsha and S. Alam, *Constr. Build. Mater.*, 309(2021)125115.
29. Z.Q. Jin, C.S. Xiong, T.J. Zhao, Y.J. Du, X.Y. Zhang, N. Li, Y. Yu and P.G. Wang, *Cem. Concr. Compos.*, 126(2022)104375.
30. H. Yang, C.S. Xiong, X.Y. Liu, A. Liu, T.Y. Li, R. Ding, S.P. Shah and W.H. Li, *Constr. Build. Mater.*, 307(2021)124991.
31. E.E. Alami, F.E. Fekak, L. Garibaldi and A. Elkhalfi, *J. Build. Eng.*, 43(2021)102789.

32. Z. Wang, K. Maekawa, H. Takeda and F.Y. Gong, *Cem. Concr. Compos.*, 123(2021)104181.
33. X.Q. Xu, D.Y. He, S.W. Zeng, W. He, H.M. Tan and Z.W. Yu, *Constr. Build. Mater.*, 293(2021)123440.
34. A. Cladera, A. Marí and C. Ribas, *Eng. Struct.*, 24(2021)113163.
35. H.T. Bui, K. Maekawa and K.H. Tan, *Constr. Build. Mater.*, 316(2022)125883.
36. Y. Wang, J.S. Jin, M. Zhang, X.Y. Wang, P. Gong, J.C. Zhang and J.C. Liu, *J. Alloys Compd.*, 858(2021)157712.
37. H. Thota, R. Jeyaraam, L.R. Bairi, A.S. Tirunilai, A. Kauffmann, J. Freudenberger, M. Heilmaier, S. Mandal and S.S. Vadlamani, *J. Alloys Compd.*, 888(2021)161500.
38. M. Zhu, B.Z. Zhao, Y.F. Yuan, S.M. Yin, S.Y. Guo and G.Y. Wei, *Mater. Chem. Phys.*, 279(2022) 125725.
39. M. Zhu, B.Z. Zhao, Y.F. Yuan, S.M. Yin and G.Y. Wei, *J. Electroanal. Chem.*, 882(2021)115026.
40. H. Luo, S.W. Zou, Y.H. Chen, Z.M. Li, C.W. Du and X.G. Li, *Corros. Sci.*, 163(2020)108287.
41. Y. Hou, J. Zhao, C.Q. Cheng, L. Zhang, J. Li, B.J. Liu and T.S. Cao, *J. Alloys Compd.*, 830(2020)154422.
42. H.T. Wang and E.H. Han, *Electrochim. Acta*, 90(2013)128.
43. W.M. Tian, N. Du, S.M. Li, S.B. Chen and Q.Y. Wu, *Corros. Sci.*, 85(2014)372.
44. M.A. Amin, XPS and SEM studies, *Electrochim. Acta*, 54(2009)1857.
45. G. Sridhar, N. Birbilis and V.S. Raja, *Corros. Sci.*, 182(2021)109276.
46. D.W. Li, R. Wei, L. Li, X.T. Guan and X.M. Mi, *Constr. Build. Mater.*, 199(2019)359.
47. Z.H. Dong, W.S. Guo, A.Z. Xing and P. Guo, *Electrochim. Acta*, 56(2011)5890.
48. C.Z. Li and K.L. Xi, *Constr. Build. Mater.*, 305(2021)124666.
49. J. Qiu, Y.H. Li, Y. Xu, A.J. Wu and D.D. Macdonald, *Corros. Sci.*, 175(2020)108886.
50. Z.H. Dong, W.S. Xing and P. Guo, *Corros. Sci.*, 53(2011)1322.
51. A. Chauhan and U.K. Sharma, *Struct.*, 19(2019)296.
52. Y.M. Tang, Y. Zuo and X.H. Zhao, *Corros. Sci.*, 50(2008)994.
53. K.K. Tang, *Corros. Sci.*, 152(2019)153.
54. A. Brenna, S. Beretta, F. Bolzoni, M.P. Pedferri and M. Ormellese, *Constr. Build. Mater.*, 137(2017)76.
55. L. Sánchez and H.B. Cong, *Eng. Failure Anal.*, 129(2021)105661.
56. A.A. Dastgerdi, A. Brenna, M. Ormellese, M.P. Pedferri and F. Bolzoni, *Corros. Sci.*, 159(2019)108160.
57. X.L. Hou, Q.Y. Ren, Y.K. Yang, X.L. Cao, J. Hu, C. Zhang, H.D. Deng, D.L. Yu, K.J. Li and W. Lan, *J. Nat. Gas Sci. Eng.*, 86(2021)103718.
58. P. Ghods, O.B. Isgor, G.A. McRae and G.P. Gub, *Corros. Sci.*, 52(2010)1649.
59. H.X. Qiao and B.R. Zhu, *J. Mater. Sci. Eng.*, 37(2019)107.
60. M. Zhu, C.W. Du, X.G. Li, Z.Y. Liu, H. Li and D.W. Zhang, *Corros. Sci.*, 87(2014)224.
61. M. Zhu, C.W. Du, X.G. Li, Z.Y. Liu, S.R. Wang, J.K. Li and D.W. Zhang, *Electrochim. Acta*, 117(2014)351.
62. V. Cruz, Q. Chao, N. Birbilis, D. Fabijanic, P.D. Hodgson and S. Thomas, *Corros. Sci.*, 164(2020)108314.
63. Y.Z. Shi, J.K. Mo, F.Y. Zhang, B. Yang, P.K. Liaw and Y. Zhao, *J. Alloys Compd.*, 844(2020) 156014.
64. Z. Zhang, X.L. Yuan, Z.Y. Zhao, X.F. Li, B. Liu and P.K. Bai, *J. Electroanal. Chem.*, 894(2021)115351.
65. L.Y. Zhu, Z.Y. Cui, H.Z. Cui, X. Wang and Y.Z. Li, *Corros. Sci.*, 23(2021)110039.
66. D. Guo, J. Chen, X. Chen, Q. Shi, V.A.M. Cristino, C.T. Kwok, L.M. Tam, H. Qian, D. Zhang and X. Li, *Corros. Sci.*, 193(2021)109887.
67. C. Pan, L. Liu, Y. Li and F.H. Wang, *Thin Solid Films*, 519(2011)4781.
68. X.Q. Yue, Y.Q. Ren, L.Y. Huang, S. Zou, L. Zhang, and Y. Hua, *Corros. Sci.*, 194(2022)109935.

69. S. Liu, H.Y. Sun, L.J. Sun, and H.J. Fan, *Corros. Sci.*, 65(2012)520.
70. W.Liu, F.Cao, A.Chen, L.Chang, J.Zhang and C.Cao, *Corrosion*, 68(2012) 045001
71. L.Y. Xu, X. Su, Z.X. Yin, Y.H. Tang and Y.F. Cheng, *Corros. Sci.*, 61(2012)215.
72. Y. Liang, Y.X. Du, D.Z. Tang, L. Chen, L. Zhang, and L.J. Qiao, *Corros. Sci.*, 197(2022)110085.
73. X.P. Wang, M.H. Shao, C.Q.Ye, S.G. Dong, R.G. Du, and C.J. Lin, *J. Electroanal. Chem.*, 895(2021)115454
74. D.Han, Y.M.Jiang, C.Shi, B.Deng, and J.Li, *J.Mater.Sci.*, 47(2012)1018.
75. Z. Wang, J. Jin, G.H. Zhang, X.H. Fan, and L. Zhang, *Corros. Sci.*, 208(2022)110611.
76. Y.W. Liu, M.R. Liu, X. Lu, and Z.Y. Wang, *Mater. Chem. Phys.*, 277(2022)124962.

© 2022 The Authors. Published by ESG (www.electrochemsci.org). This article is an open access article distributed under the terms and conditions of the Creative Commons Attribution license (<http://creativecommons.org/licenses/by/4.0/>).